

Supplementary Information for:

Environmentally robust *cis*-regulatory changes underlie rapid climatic adaptation

Mallory A. Ballinger, Katya L. Mack, Sylvia M. Durkin, Eric A. Riddell, and
Michael W. Nachman

Mallory Ballinger, Michael Nachman
Email: mallory.ballinger@berkeley.edu; mnachman@berkeley.edu

This PDF file includes:

Supplementary text

Figs. S1 to S14

Tables S1 to S3

Legend for Dataset S1

SI References

Other supplementary materials for this manuscript include the following:

Dataset S1

Supporting Information Text

EXPANDED MATERIALS and METHODS:

Pelage Conductance

We measured the thermal conductance of pelage from house mouse specimens (i.e., ‘flat skins’; $n = 32$ per line) to determine differences between populations from New York and Brazil. We sacrificed experimental mice and then air dried the specimens for at least two weeks until completely dry. We used a device that combines a heat flux transducer with controlled heat dissipation across flat skin specimens to measure the thermal conductance of the pelage (see Riddell et al. 2021 for a detailed explanation of methods).

Briefly, the device consisted of a copper pipe (2.54 cm in diameter) that circulated warm water controlled at 37°C to simulate the normothermic body temperature of small mammals. The water was circulated through the pipe using a submersible water pump (Aquatop, N-302) from a temperature-controlled bath into the copper pipe. The copper pipe was embedded into a 6-inch cube of polystyrene to minimize heat transfer away from the pipe, and the tip of the copper pipe was flush with the foam insulation to direct the flow of heat from the warm copper pipe into the flat mammal skin positioned on top of the copper pipe. Between the copper pipe and specimen, we placed a heat flux sensor (FluxTeq, PFHS-01) on top of the copper pipe and secured using double-sided tape. The heat flux sensor (surface area = 1.6 cm²) was a differential-temperature thermophile made of Kapton (polyimide) with a sensor thickness of approximately 305 microns. The heat flux sensor contains a type-T thermocouple embedded into the sensor to simultaneously measure heat flux (W m⁻²) and temperature (°C) across the sensor surface. Then, we applied a thin layer of petroleum jelly (Vaseline™) to the skin on the underside of the specimen to ensure that the skin was sealed to the heat flux sensor without any air pockets (1). We then clamped the edges of the specimen to further ensure a lack of air pockets using DeWalt® Trigger Clamps while also not disrupting the section of pelage being measured. At the tips of the pelage, we placed a precision wire type-T probe thermocouple (Thermoworks, PT-6; gauge = 0.07366 cm) using an alligator clip to measure the temperature gradient across the mammal pelage. The entire apparatus was placed inside a temperature-controlled incubator chamber (ReptiPro 6000) held at 30°C.

We recorded the heat flux and temperature from various thermocouples using an analog voltage measurement system (FluxTeq, FluxDAQ) with an integrated thermistor for cold junction temperature compensation. The FluxDAQ continuously measured the temperature of the copper pipe, heat flux across the copper pipe into the skin, temperature above the pelage, air temperature, and wall temperature of the incubator. We used air temperature and wall

temperature measurements to ensure black-body conditions within the chamber (1). We measured a single estimate of conductance across the dorsal midline of each specimen, with each measurement taking roughly 30 – 45 m to come to thermal equilibrium. After the readings had come to equilibrium, we recorded the average conductance value over 90 s. We then calculated thermal conductance ($\text{W m}^{-2} \text{ }^{\circ}\text{C}^{-1}$) by dividing the heat flux from the heat flux transducer (W m^{-2}) by the difference in temperature ($^{\circ}\text{C}$) between the heat flux transducer and tip of the pelage (2).

Genotype-by-Sex Patterns

To determine the effects of sex on gene expression evolution, we quantified genotype-by-sex interactions (GxS) by fitting a generalized linear model following a negative binomial distribution using DESeq2 (Love et al. 2014). Specifically, we determined the effects of genotype, sex, and genotype-by-sex on expression patterns for each tissue and temperature treatment, separately. We removed genes with fewer than an average of 10 reads per individual within each tissue. We used a Benjamini-Hochberg multiple test correction (Benjamini and Hochberg, 1995) on the resulting *P*-values and considered genes with a false discovery rate (FDR) smaller than 0.05 to be significantly differentially expressed.

Sex-Specific Gene Regulatory Patterns

Males were used to assign regulatory categories to maximize power due to a larger number of hybrid samples sequenced (6 replicates of F1 males vs. 4 replicates of F1 females). Sex-specific allele-specific expression was identified for autosomal genes in DESeq2 under the model ~sex + individual:sex + allele:sex by contrasting male:allele and female:allele based on a randomly chosen equal number of male and female F1s. To identify trans*sex interactions, we fit a model that included parental and hybrid read counts (~allele + allele:generation + population:sex + population:generation:sex) for each tissue separately for autosomal genes.

EXPANDED RESULTS:

Pervasive Expression Divergence Despite Genotype-by-Sex Interactions

Although males and females showed similar patterns of gene expression evolution, we asked whether differences in sexual dimorphism in gene expression also played a role in expression divergence between New York and Brazil. To characterize the role of genotype-by-sex interactions in expression divergence, we identified genotype-by-sex interactions (GxS) for each tissue and environment separately. Consistent with strong patterns of divergence, the vast majority of genes showed differential expression between New York and Brazil mice, regardless of sex (Figure S4). Interestingly, however, BAT harbored very little GxS compared to liver

(Figure S4). When we examined sample-to-sample distances with hierarchical clustering, BAT samples indeed clustered strongly by genotype but not by sex (Figure S14).

Sex-Specific Regulatory Divergence between New York and Brazil

To understand the relative contribution of sex differences to *cis*- and *trans*- regulatory divergence between New York and Brazil, we compared the differences in effect sizes between males and females (i.e., average | male effect size *cis* - female effect *cis* | vs. average | male effect size *trans* - female effect size *trans* |). Sex was found to have a larger average effect on *trans* divergence in both tissues ($p < 2.2\text{e-}16$). Next, we investigated genes for sex-specific allele-specific expression. We found limited evidence for sexually dimorphic gene regulatory divergence between lines. Contrasting allelic expression between males and females, we identified 22 autosomal genes in the liver and 11 genes in BAT with sexually dimorphic allele-specific expression (FDR<0.1). Six of these genes showed sexually dimorphic allele-specific expression in both tissues (*ebpl*, *ddx55*, *fh1*, *tmed2*, *spata13*, *C130074G19Rik*). Comparing expression between male and female individuals of the parental and hybrid generation, we also identified 26 autosomal genes with a significant effect of sex on *trans*- divergence (FDR<0.1).

Supplemental Figures:

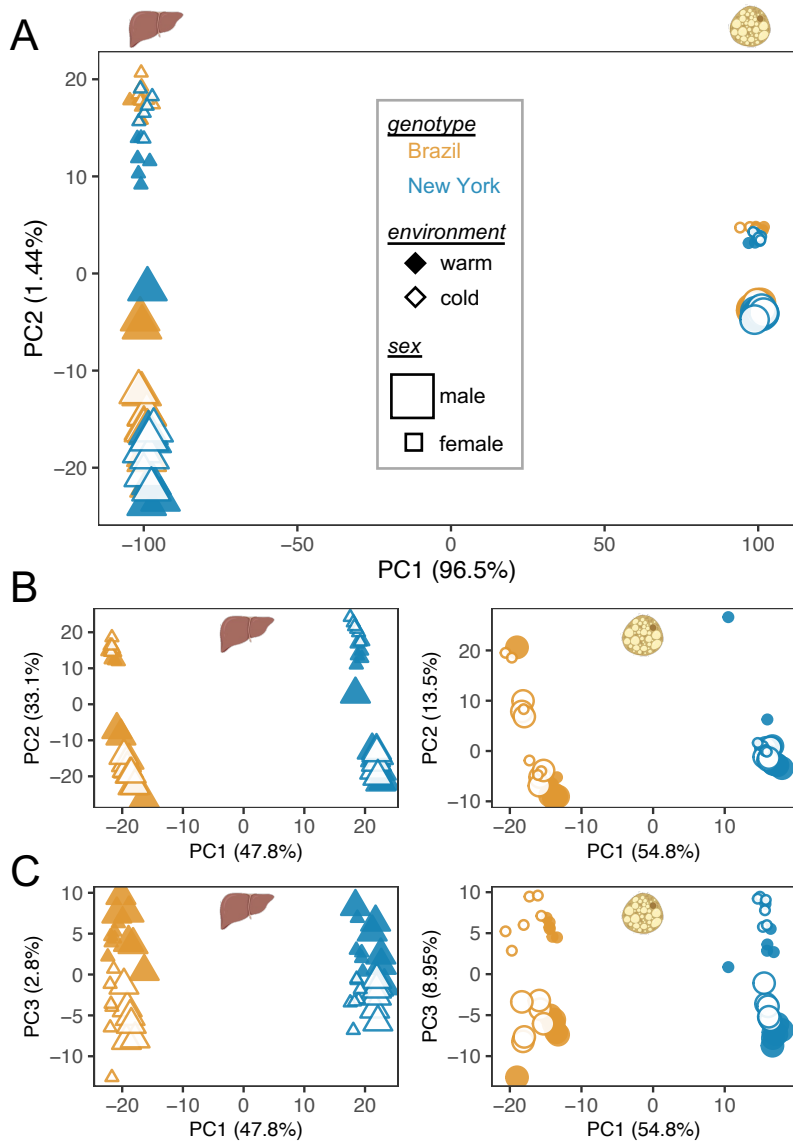


Figure S1: Principal components analysis explaining expression level variation of Brazil and New York mice across tissue, sex, and environment. (A) When analyzing all expression data together, PC1 explains ~97% of the variance and reflects tissue-type, while PC2 explains ~1.5% of the variance and reflects differences in sex. (B) When analyzing expression data for each tissue separately, PC1 explains ~50% of the variance and reflects genotype differences for both tissues. While no clear patterns are observed across PC2, (C) PC3 explains ~3% of the variance in liver and reflects differences in environment. In BAT, PC3 explains ~9% of the variance and reflects differences in sex.

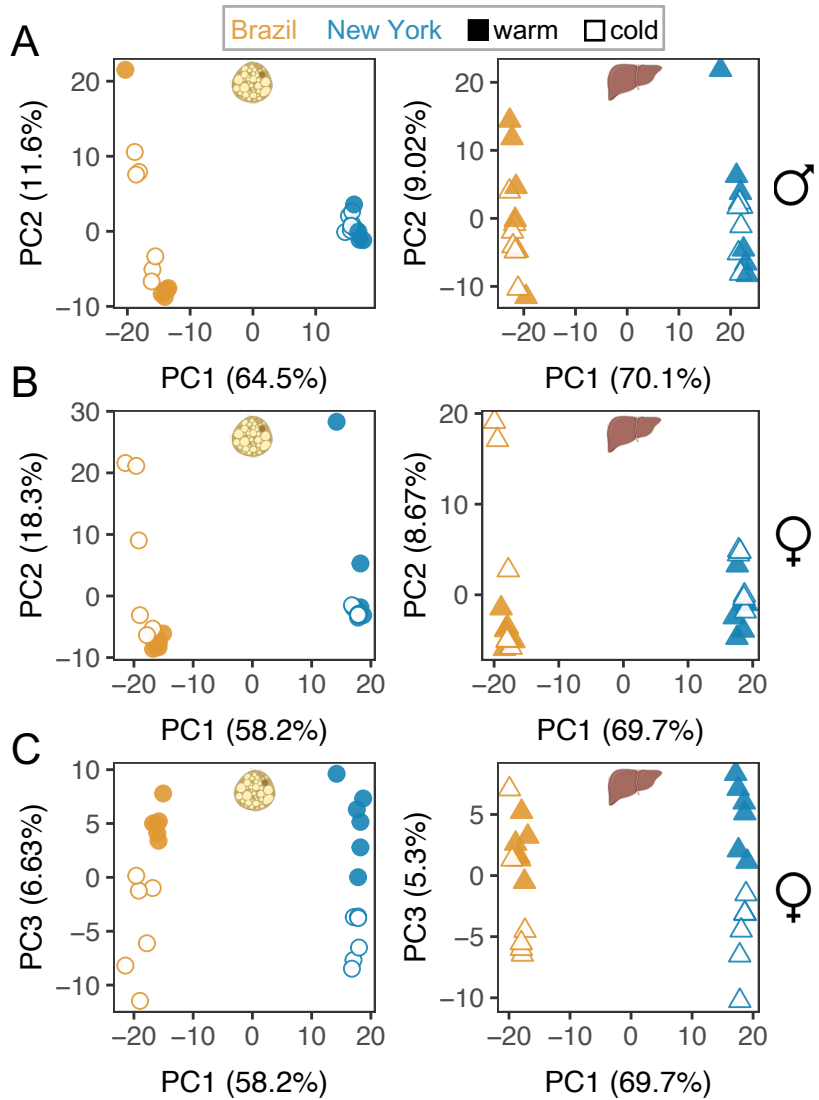


Figure S2: Principal components analysis explaining expression level variation of Brazil and New York mice across environment for tissue-type and sex, separately. While PC1 explains roughly 60% of the variance in both male (A) and female (B) gene expression (and reflects genotype differences), PC2 does not clearly separate individuals by environment. (C) In females, PC3 explains > 5% of the variance in both tissues, and largely separates out samples based on environment across both tissues.

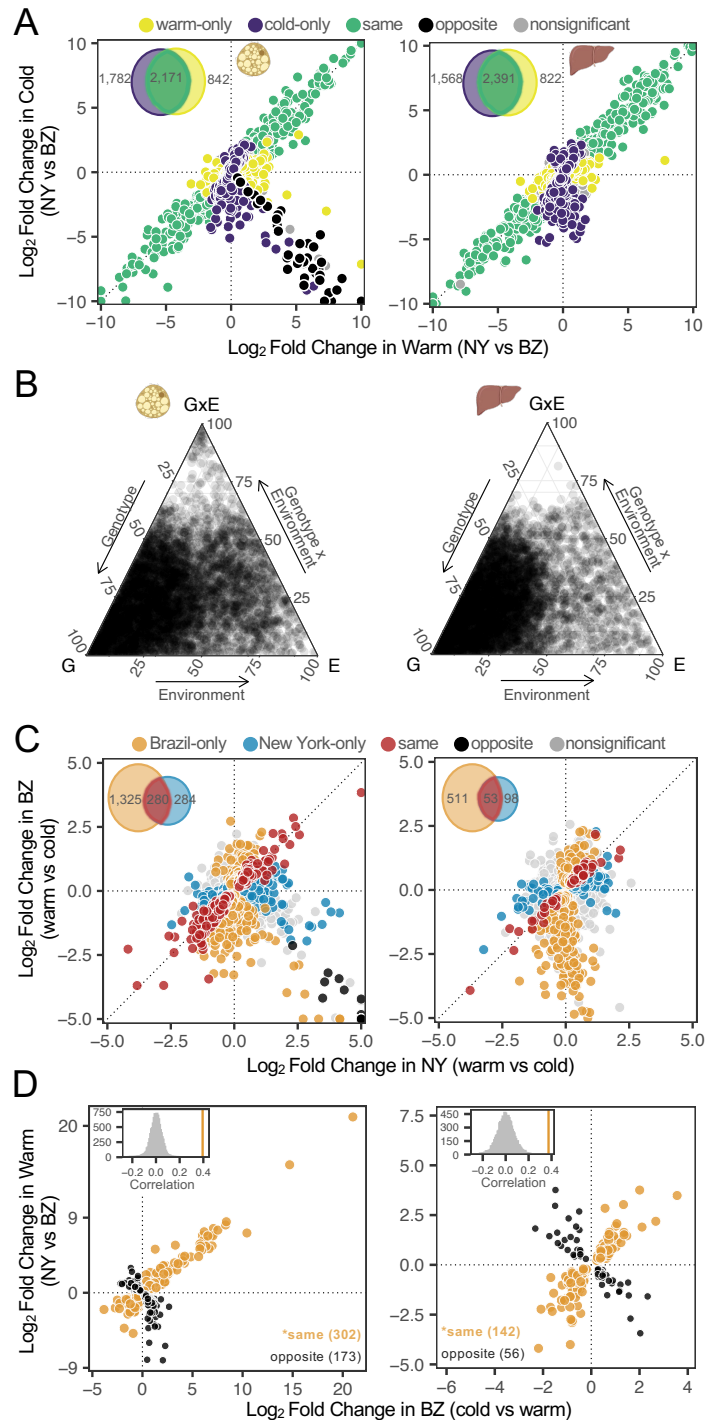


Figure S3: Divergence and GxE patterns in females. (A) Expression divergence between temperature-regimes in BAT and liver. Log2 fold changes between parents were calculated for all genes independently. In each panel, genes (points) are colored depending on their direction and significance of the log2 fold change (FDR < 0.05). (B) Ternary plots depicting the proportion of each gene's expression variance explained by genotype (G), environment (E), and GxE. The relative proportion of each factor is shown for all differentially expressed male genes in BAT

and liver. Total variance is the sum of all three components. **(C)** Comparison of gene expression differences between temperature regimes in NY and BZ females in both BAT and liver. Log₂ fold changes between temperatures were calculated for all genes independently. In each panel, genes (points) are colored depending on their direction and significance of the log₂ fold change. GxE categories include line-specific responses or opposite responses between lines. Insets depict the total number of differentially expressed genes for each comparison (FDR < 0.05). **(D)** The relationship between plasticity of gene expression and evolved divergence in gene expression in BAT and liver. Each gene (point) represents expression differences with statistically significant plasticity in Brazil (cold vs warm; FDR < 0.05) as well as significant expression divergence between NY and BZ at warm temperature (FDR < 0.05). Points colored in orange represent genes with a positive correlation between plasticity and evolved divergence and represent adaptive plasticity. Points in black represent genes with a negative association and represent non-adaptive plasticity. Insets depict the observed correlation coefficient (orange solid lines) are more positive than a randomized distribution of correlation coefficients for each tissue (see Methods for details). Asterisks denote significance of adaptive plasticity for each tissue (binomial exact tests, $P < 0.05$).

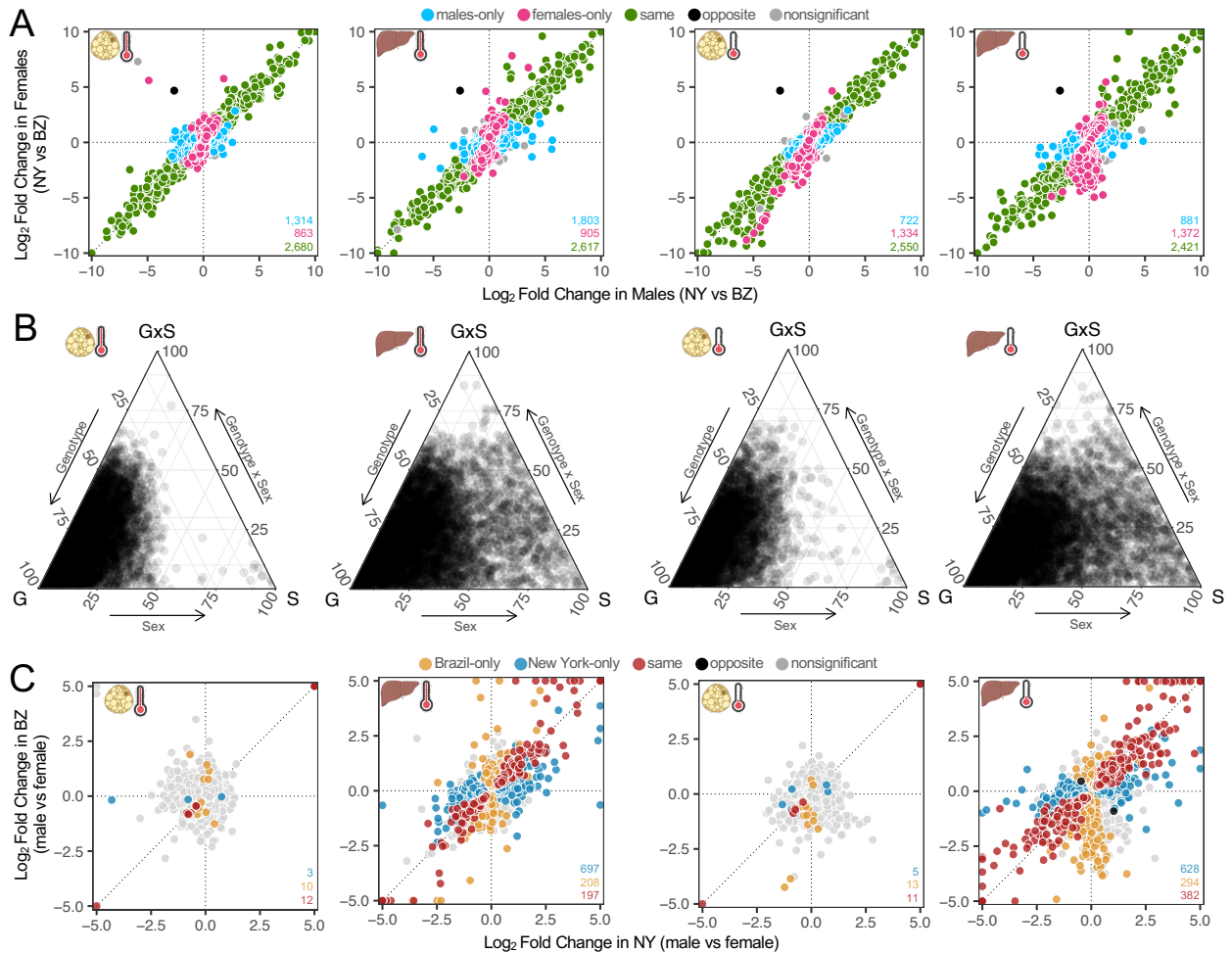


Figure S4: Parental expression patterns of divergence and genotype-by-sex interactions (GxS).

(A) Expression divergence between New York and Brazil across males and females (both tissues and temperature treatments). Log2 fold changes between parents were calculated for all genes independently. In each panel, points (representing individual genes) are colored depending on their direction and significance of the log2 fold change (FDR < 0.05). Insetted numbers portray the total number of differentially expressed genes for each comparison (FDR < 0.05). **(B)** Ternary plots depicting the proportion of each gene's expression variance explained by genotype (G), sex (S), and GxS. The relative proportion of each factor is shown for all differentially expressed genes in BAT and liver across both temperature treatments. Total variance is the sum of all three components. **(C)** Comparison of gene expression differences between sexes in NY and BZ mice in both BAT and liver and across both temperature treatments. Log2 fold changes between sexes were calculated for all genes independently. In each panel, points are colored depending on their direction and significance of the log2 fold change. GxS categories include line-specific responses or opposite responses between lines. Insetted numbers portray the total number of differentially expressed genes for each comparison (FDR < 0.05).

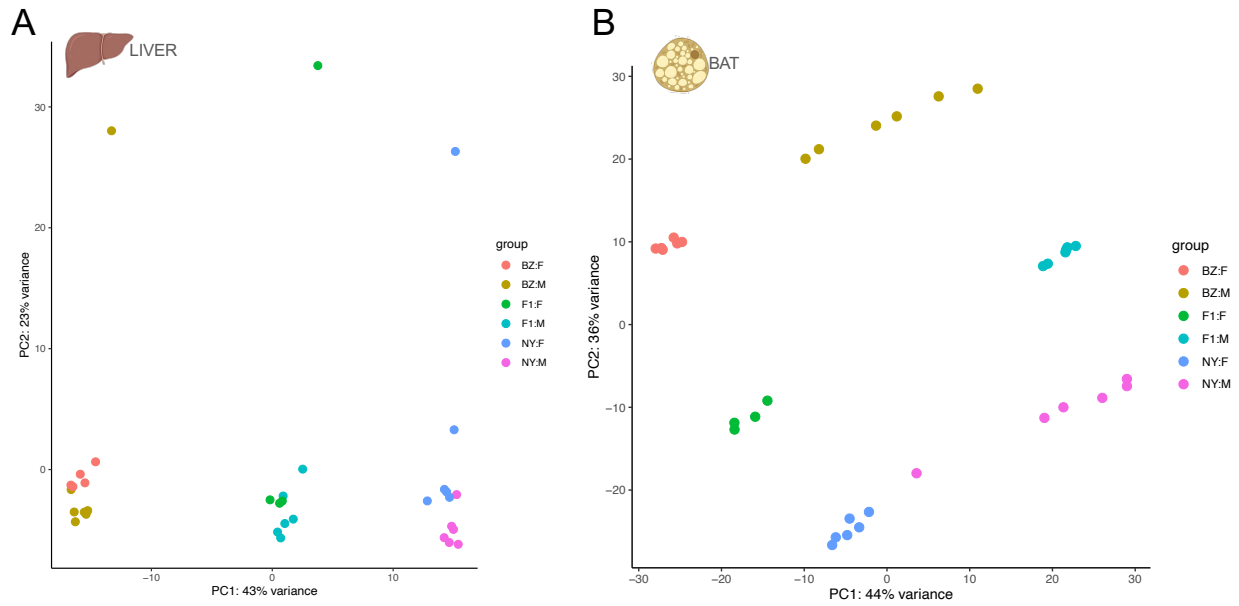


Figure S5: Principal components analysis explaining expression level variation of Brazil, New York, and F1 hybrid mice for each tissue separately. For both tissues, PC1 explains > 40% of the variance, and in the liver (A), PC1 also cleanly separates out individuals by genotype. (B) PC2 explains ~36% of the variance in BAT and largely separates out individuals by genotype.

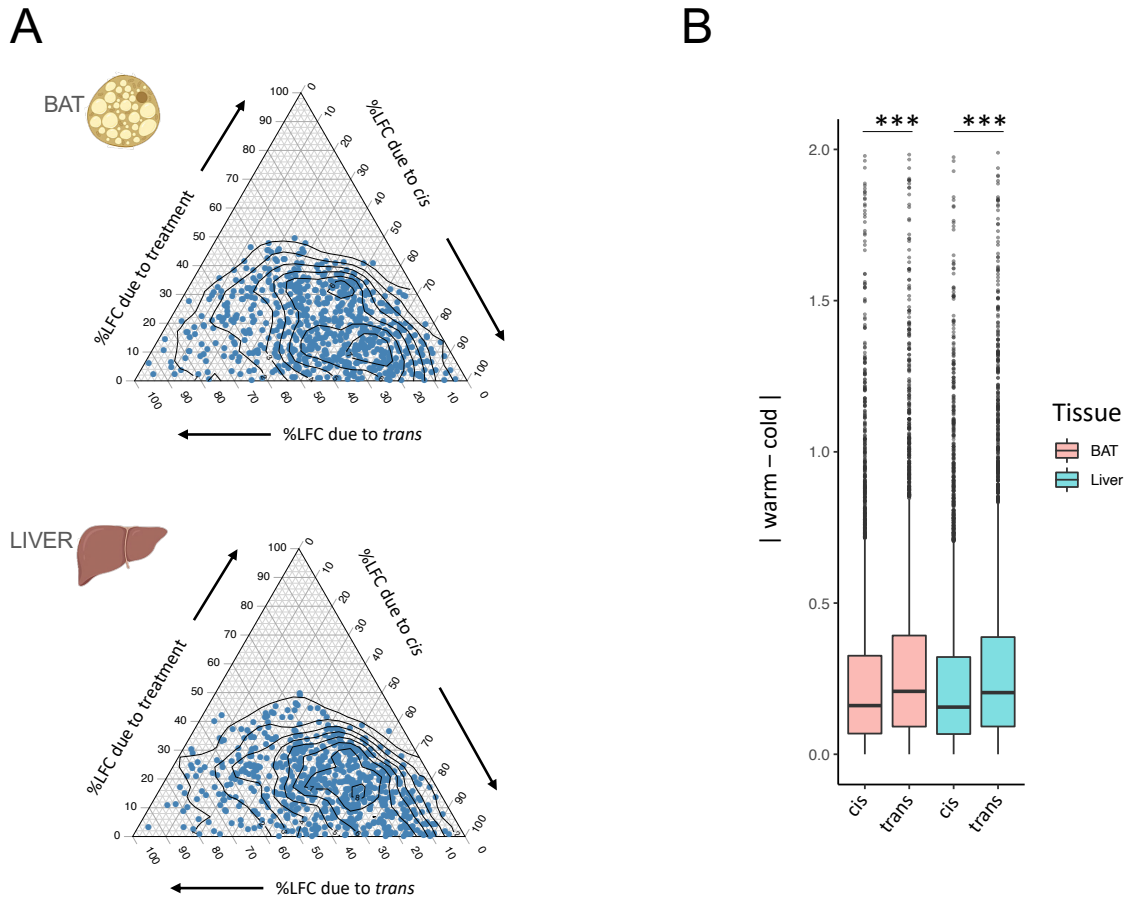


Figure S6. Effects sizes of *cis*- and *trans*- changes between environments for both BAT and liver. (A) The relative proportions of log₂-fold change due to *cis*, *trans*, and temperature for genes with significant genetic effects (*cis* and/or *trans*) in BAT and liver. Total variance is the sum of all three components. **(B)** Boxplots displaying absolute log₂-fold change of *cis*- and *trans*-difference between warm and cold environments, with *trans*- difference being greater across environments for both tissues (Wilcoxon signed-rank tests, ***P < 0.001).

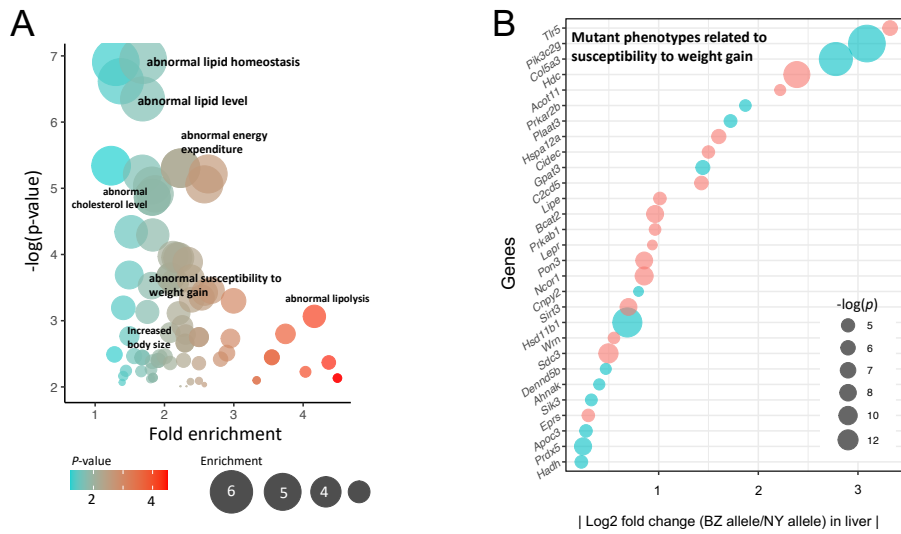


Figure S7: Enrichment of cis-regulatory changes in the liver. **(A)** Enrichmentt plot depicting liver genes with *cis*-regulatory changes for various mutant phenotype annotation for homeostasis and metabolism. **(B)** Candidate liver genes that show *cis*-changes and have a 2-fold enrichment with mutant phenotypes related to susceptibility to weight gain. Size of circle denotes significance while color of circle denotes higher expression of either BZ allele (blue) or NY allele (red).

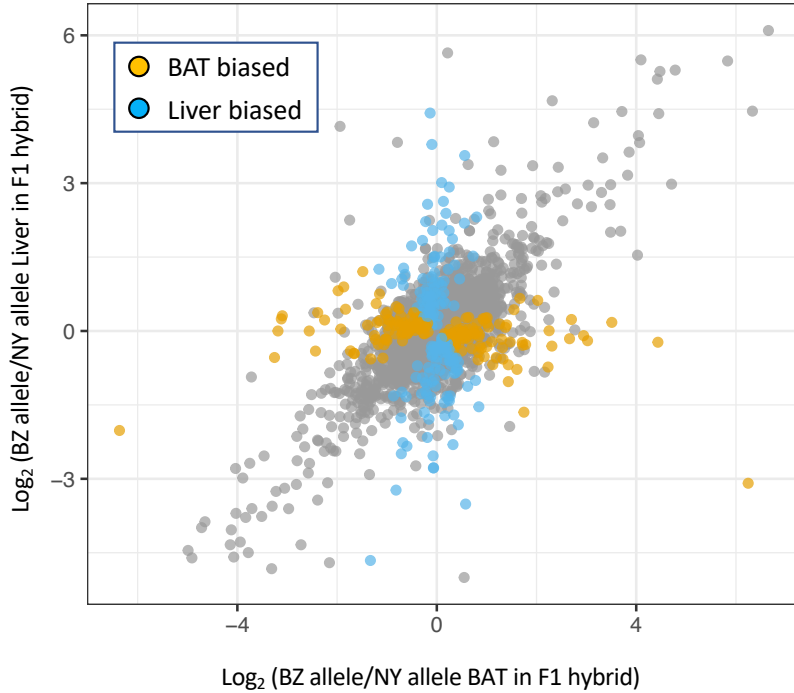


Figure S8: Tissue-dependent allele-specific expression. Scatterplot comparing the distribution of allelic ratios between BAT and liver. Points (representing individual genes) are colored by binned diffASE *P*-values on Brazil and New York allele counts in the two tissues (BAT-biased = yellow; liver-biased = blue).

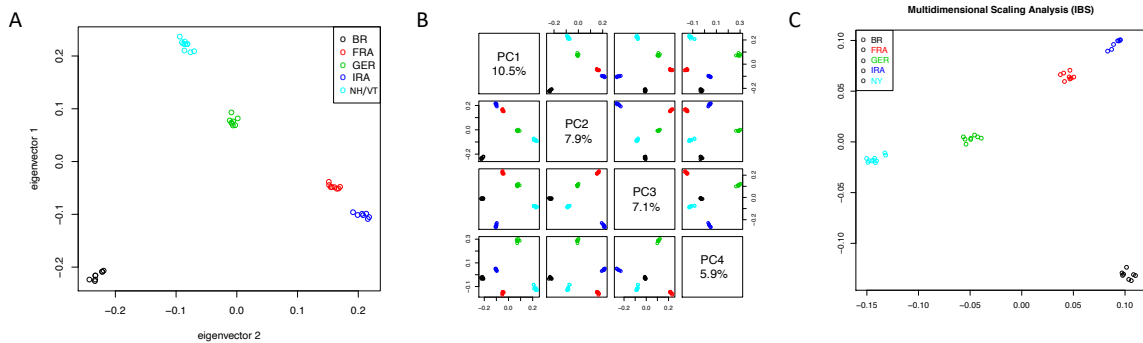


Figure S9: Genetic relationships between five populations of wild house mice. (A-B)

Genomic principal component analysis (PCA) across multiple PCs distinguishes mouse populations based on population-of-origin. (C) Multidimensional Scaling Analysis (hierarchical clustering) shows similar results to PCA, distinguishing mouse populations based on population-of-origin. Legend: BR = Brazil (black); FRA = France (red); GER = Germany (green); IRA = Iran (dark blue); NH/VT = New Hampshire / Vermont (light blue).

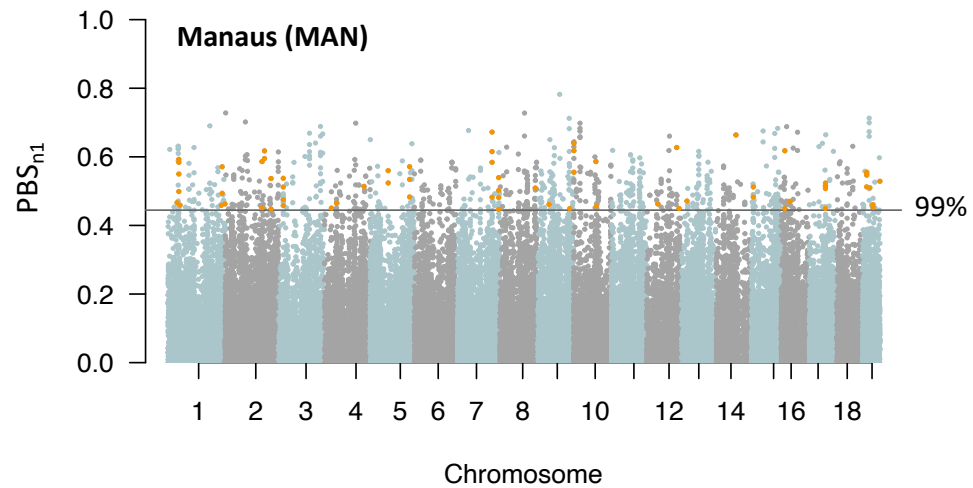


Figure S10: Autosomal selection scan showing *PBSn1* results for the Manaus (MAN) focal population. Orange points depict genes that exhibit *cis*-regulatory divergence and overlap with outlier regions.

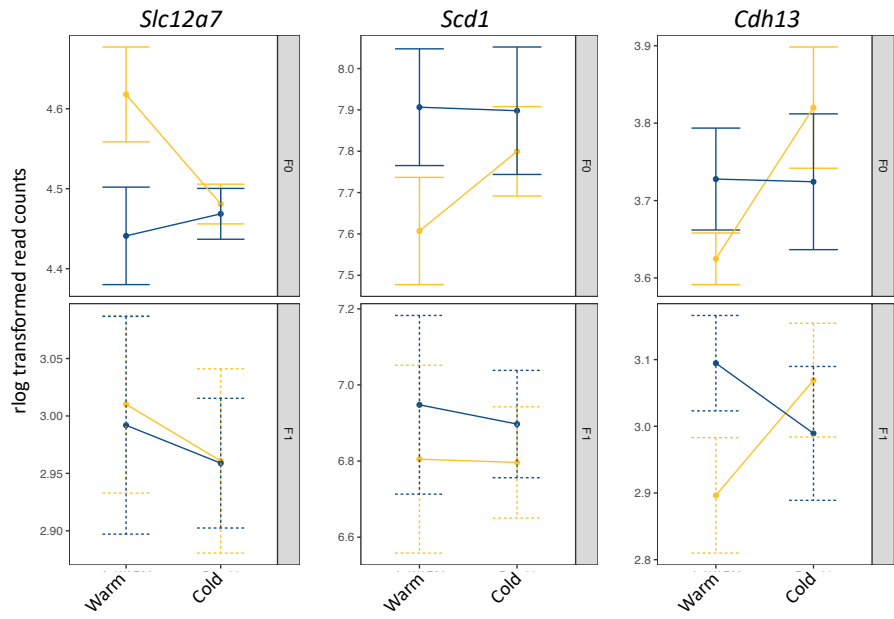


Figure S11. Expression patterns of three candidate genes showing adaptive plasticity and significant (A) *trans* x environment interactions, (B) *cis* x environment interaction, and (C) *cis* + *trans* x environment interactions. Parental expression (F0) and allelic expression (F1) are plotted as regularized log transformed counts.

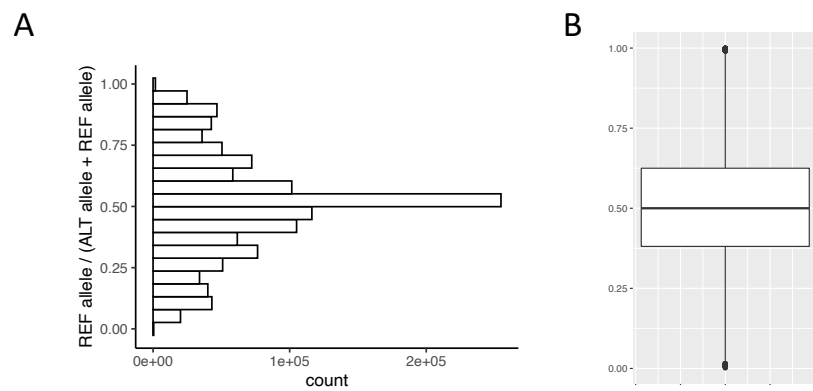


Figure S12. No evidence for reference mapping bias. (A) Distribution of reads overlapping the references vs. alternative allele (REF allele / (ALT allele + REF allele)). (B) These proportions show a median of 0.5 across samples.

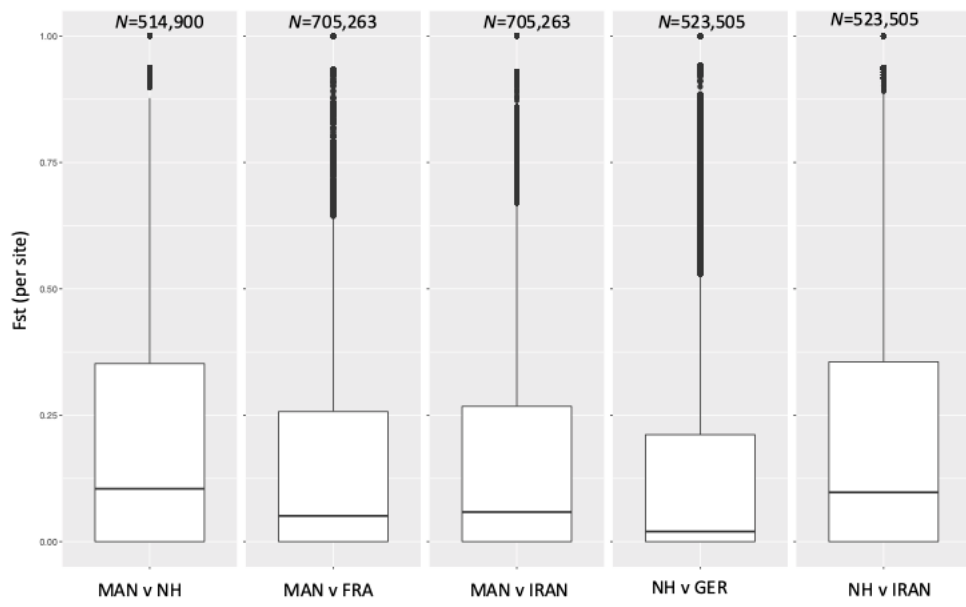


Figure S13: Pairwise Fst (per site) of *M.m. domesticus* populations used in *PBSn1* analysis.

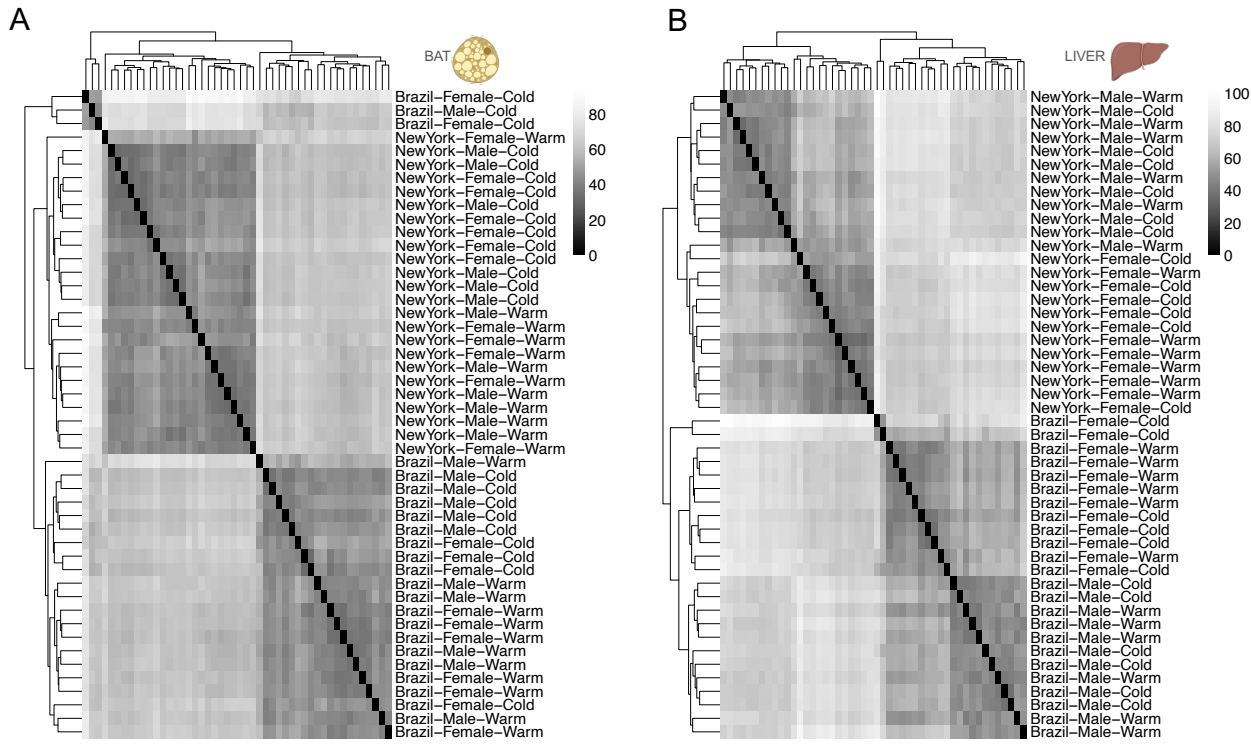


Figure S14. Hierarchical clustering of sample-to-sample distances in (A) BAT and (B) liver.

For both tissues, samples largely cluster by genotype. However, in BAT, samples do not cluster by sex.

Supplemental Tables

Table S1. Results of linear mixed models investigating the effects of sex and genotype (line) on body mass, pelage conductance, and extremity length in house mice.

Trait	Factor	χ^2	DF	P-value	Effect size (ω^2)
Body Mass (g)					
	Line	28.54	1	< 0.001	0.48
	Sex	15.29	1	<0.001	0.31
Pelage Conductance ($\text{W}^{-1}\text{m}^{-2}\text{C}^{-1}$)					
	Line	21.65	1	< 0.001	0.35
	Sex	0.05	1	0.82	-0.03
Relative Tail Length (mm/g)					
	Line	85.97	1	< 0.001	0.74
	Sex	12.12	1	< 0.001	0.26
Relative Ear Length (mm/g)					
	Line	66.67	1	< 0.001	0.73
	Sex	18.55	1	< 0.001	0.35

Table S2. Genes with significant *trans* x temperature effects for each tissue.

Tissue	Gene Symbol	Ensembl Number
BAT		
	<i>arl6ip6</i>	ENSMUSG00000026960
	<i>hsd11b1</i>	ENSMUSG00000016194
	<i>parm1</i>	ENSMUSG00000034981
	<i>wnt11</i>	ENSMUSG00000015957
	<i>gstt1</i>	ENSMUSG00000001663
	<i>cdh13</i>	ENSMUSG00000031841
	<i>tmem45b</i>	ENSMUSG00000041737
	<i>prpf40a</i>	ENSMUSG00000061136
	<i>ccdc3</i>	ENSMUSG00000026676
	<i>xylt1</i>	ENSMUSG00000030657
	<i>amy1</i>	ENSMUSG00000074264
	<i>erbb2</i>	ENSMUSG00000062312
	<i>itih5</i>	ENSMUSG00000025780
	<i>adamts9</i>	ENSMUSG00000030022
	<i>sec14l4</i>	ENSMUSG00000019368
	<i>slc14l4</i>	ENSMUSG00000017756
	<i>fam111a</i>	ENSMUSG00000024691
	<i>arhgef10</i>	ENSMUSG00000071176
Liver		
	<i>hmgs2</i>	ENSMUSG00000027875

Table S3. Genes with ASE that co-localize with genomic outliers for NH/VT and are candidates for metabolic adaptation based on mutant phenotypes.

Gene	Mutant Phenotypes
<i>Col6a1</i>	body weight and size; metabolism (glucose tolerance) body weight; body fat composition; diet-induced obesity; energy expenditure; food intake; body temperature; metabolism (e.g., cholesterol, leptin, triglyceride levels)
<i>Prkar2b</i>	body weight; diet-induced obesity; metabolism (e.g., glucose tolerance, insulin levels)
<i>Sulf2</i>	body weight and size
<i>Enpp3</i>	susceptibility to weight loss
<i>Smoc1</i>	body weight and size; body fat; activity level
<i>Myo10</i>	body weight and size
<i>Prkdc</i>	body size and weight gain
<i>Stard4</i>	body weight and size; metabolism (cholesterol level) body weight and size; diet-induced obesity; food intake; fat composition; body temperature; metabolism (e.g., glucose level, insulin sensitivity)
<i>Impact</i>	body weight; body fat composition; food intake; metabolism (e.g., triglyceride, lipid, cholesterol level, insulin resistance)
<i>Lipa</i>	body weight
<i>Als2</i>	body weight and size
<i>Col5a2</i>	body size
<i>Col3a1</i>	weight gain
<i>Mpzl1</i>	postnatal growth
<i>Stam</i>	body weight; diet-induced obesity; body fat composition; energy expenditure; body temperature; metabolism (e.g., leptin, adiponectin, glucose, insulin levels)
<i>Bcat2</i>	postnatal growth
<i>Stim1</i>	susceptibility to age related obesity; body fat composition; metabolism (e.g., triglyceride, cholesterol, insulin levels)
<i>Wrn</i>	body weight; postnatal growth
<i>Ets1</i>	body size; activity level; metabolism (e.g., glucose, triglyceride level)
<i>Myo6</i>	body weight
<i>Tpst1</i>	body weight
<i>Sbno2</i>	body weight; postnatal growth
<i>Cc2d2a</i>	body weight; postnatal growth

<i>B3glct</i>	body size susceptibility to weight gain; body fat composition; susceptibility to diet-induced obesity; metabolism (e.g., leptin, adiponectin, glucose levels)
<i>Plaat3</i>	body weight; susceptibility to diet-induced obesity; body fat composition; metabolism (e.g., glucose tolerance)
<i>Ahnak</i>	lean body mass
<i>Cog1</i>	body size; body fat amount; metabolism (insulin level, glucose tolerance)
<i>Tmem106b</i>	body fat amount; activity
<i>Vps13a</i>	Activity level; metabolism (glucose level)
<i>Wwp1</i>	Activity level; lean body mass; metabolism (glucose tolerance)
<i>Dhx29</i>	Metabolism (glucose level)
<i>Sypl</i>	Activity level; metabolism (glucose level)
<i>Arhgef10</i>	metabolism (e.g., cholesterol, triglyceride level)
<i>Gpr146</i>	metabolism (e.g., triglyceride level)
<i>Rsad1</i>	metabolism (e.g., cholesterol level)
<i>Pctp</i>	metabolism (e.g., cholesterol level, lipid homeostasis)
<i>Uaca</i>	metabolism (cholesterol level)
<i>Slc46a3</i>	activity, metabolism (cholesterol level)
<i>Uaca</i>	metabolism (cholesterol level)
<i>Cd44</i>	metabolism (lipid level)
<i>Mmd</i>	body size; activity
<i>Zfyve1</i>	body size

SI Dataset S1 (Data_S1.xlsx)

Individual metadata and candidate genes. This file includes:

Sheet 1: Phenotypic metadata for SARA and MANA

Sheet 2: Metadata for RNA-seq samples and associated MVZ accession numbers

Sheet 3: Genes overlapping PBSn1 outlier blocks in New Hampshire / Vermont
(NH/VT)

Sheet 4: Genes overlapping PBSn1 outlier blocks in Manaus (MAN)

Sheet 5: Genes with ASE overlapping PBSn1 outliers in both MAN and NH/VT

Sheet 6: Phenotype enrichments of outlier genes with ASE in both warm and cold
in NH/VT

SI References

1. GE Walsberg, GS Campbell, JR King, Animal coat color and radiative heat gain: A re-evaluation. *J. Comp. Physiol. B* **126**, 211–222 (1978).
2. GE Walsberg, Heat flow through avian plumages: The relative importance of conduction, convection, and radiation. *Journal of Thermal Biology* **13**, 89–92 (1988).